

www.acsami.org Research Article

Tailoring Electrical Properties in Carbon Nanomaterial Patterns with Multimaterial Aerosol Jet Printing

Livio Gamba, Moham Ed Abdur Razzaq, Santiago Diaz-Arauzo, Mark C. Hersam, Xianglan Bai, and Ethan B. Secor*



Cite This: ACS Appl. Mater. Interfaces 2023, 15, 57525-57532



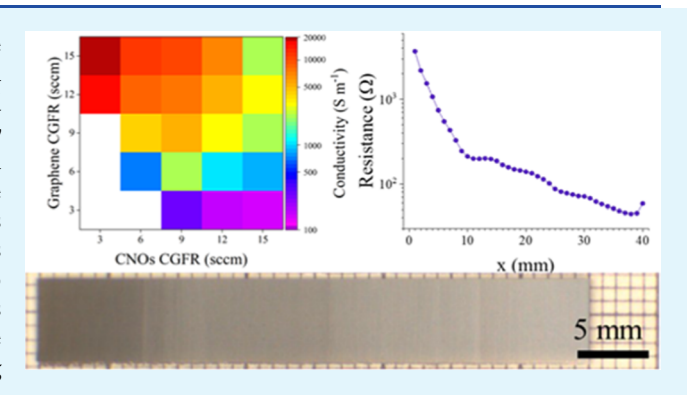
ACCESS I

III Metrics & More

Article Recommendations

s Supporting Information

ABSTRACT: Multimaterial aerosol jet printing offers a unique capability to freely mix inks with different chemical compositions in the aerosol phase, enabling one-step digital fabrication with tailored compositions or functionally graded structures, including in the x-y plane. Here, in situ mixing of two carbon nanomaterial inks with distinct electrical properties is demonstrated. By tailoring the mixing ratio of the constituent inks, electrical conductivity is modulated by $130\times$, and sheet resistance values for a single pass span approximately 2 orders of magnitude. The ability to manufacture components with tailored electrical properties offers significant value for hybrid and flexible electronic device applications, such as microelectronics packaging. Moreover, grading properties within a part provides a new dimension of design freedom for complex assemblies.



KEYWORDS: printed electronics, multimaterial printing, functionally graded materials, advanced manufacturing, hybrid electronics

INTRODUCTION

Functionally graded materials (FGMs) are characterized by spatially inhomogeneous chemical composition, which yields properties distinct from those of the pure constituents and thus supports advanced applications of customizable parts. Because of these advantages, FGMs have been the subject of numerous studies for applications in the areas of aerospace, structural design,² biomedical devices,³ and electronics.^{4–8} Specifically, within the electronics industry, the growing complexity of devices, which involves the meticulous integration of various materials and interfaces, places substantial demands on both design and manufacturing processes.9 For example, these requirements can include engineering tolerance for thermal expansion, 10 mitigating stresses at interfaces, 11 grading dielectric properties to engineer antennas and RF response, and engineering lithiophilicity in batteries to prevent dendriteinduced shorting. Although several techniques exist for processing different classes of graded materials, such as vapor deposition, 12 powder metallurgy, 13 and wet methods, 14 additive manufacturing offers unique advantages with precise digital control of composition and integration with lateral patterning.^{6,15} In particular, multimaterial aerosol jet printing (AJP) allows the fabrication of high-resolution composite traces by mixing multiple aerosol streams in situ during deposition. 6,8,15–17 In contrast to liquid-phase AM methods, mixing in the aerosol phase involves a low volume of active material within the mixing chamber, allowing the ratio to be

modulated within a single printing cycle with a limited delay. This is particularly important in instances where in-plane material grading is needed, as more traditional methods only support compositional grading through a film thickness via multilayer stacking 7,18 or diffusion-driven processes. 19 Nascent demonstrations of multimaterial AJP establish it as a viable framework for combinatorial patterning and on-demand material property tuning, 16,20 but development of matched inks for high-quality mixing, smooth grading, and a better understanding of patterning behavior and limitations remains a challenge with broad application potential.

In the present work, we demonstrate spatial tailoring of electrical properties in carbon nanomaterial prints using multimaterial AJP. Two distinct carbon nanomaterials, namely, graphene and carbon nano-onions (CNOs), are formulated into inks and mixed in the aerosol phase during patterning. Although these nanomaterials both nominally possess carbon and share similarities in their surface chemistry, they exhibit distinct electrical properties and morphology. The similarity in surface chemistry supports a matched solvent

Received: October 9, 2023 Revised: November 17, 2023 Accepted: November 27, 2023

Published: December 4, 2023





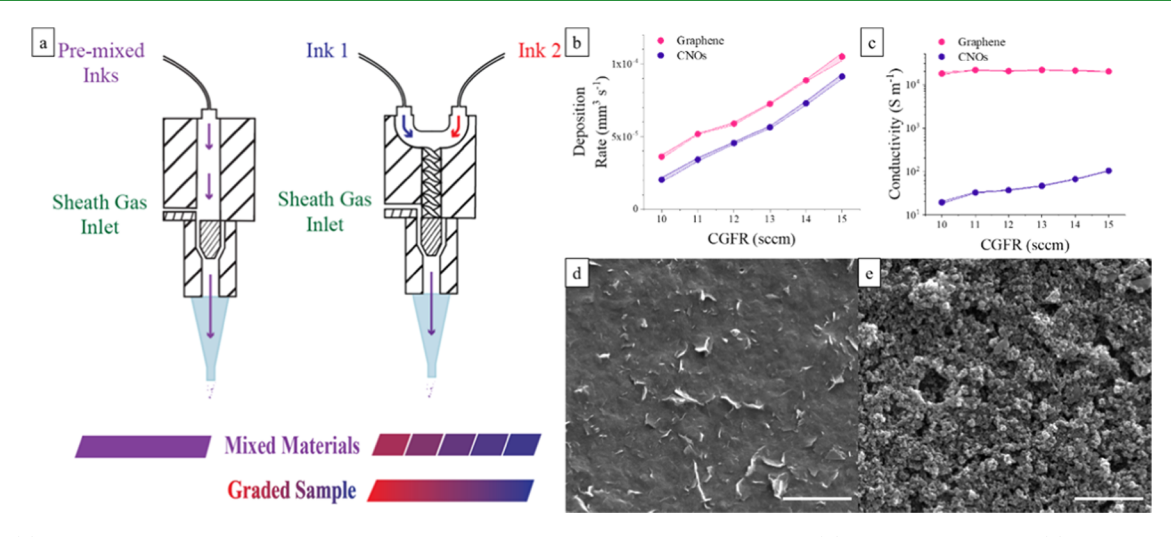


Figure 1. (a) Print characteristics of the individual graphene and CNO inks deposited separately. (b) Deposition rate and (c) conductivity data for graphene and carbon nano-onion inks printed at different carrier gas flow rates and a focusing ratio of 5, with the data standard deviation plotted as the shaded area between each data point. (d) SEM images of representative graphene and (e) carbon nano-onion samples printed on glass. Scale bar: 2 μm for both images.

and binder system, which mitigates enthalpic effects that could prevent effective blending.²³ Following benchmark evaluation of the individual inks, a series of composite inks are formulated with a controlled ratio of graphene and CNOs to evaluate modulation of electrical properties. Subsequent multimaterial AJP experiments investigate in situ mixing of the aerosol species at fixed aerosol carrier gas flow rates, demonstrating the ability to tailor electrical properties within a statically mixed material. Finally, a graded sample was fabricated in which the flow rates of individual inks were varied in small increments during deposition with Raman spectroscopy and electrical characterization, showing different composition signatures and electrical properties as a function of position. The reported results demonstrate a one-step fabrication platform to manufacture complex 2D components, with potential applications in RF engineering^{6,8} and biomedical sensing,^{24,25} among others.^{26,27}

MATERIALS AND METHODS

Materials. Ink solvents (diglyme, isobutyl acetate, and dihydrolevoglucosenone, hereafter termed Cyrene), along with the dispersant ethyl cellulose (EC, 4 cP), were purchased from Millipore Sigma (St. Louis, MO). Nitrocellulose (NC) was obtained from Scientific Polymer Products (Ontario, NY), and glycerol was purchased from Fisher Scientific (Waltham, MA). Graphene powders coated with ethyl cellulose, in which graphene comprises 30 wt % of the total powder, were prepared via liquid-phase exfoliation in a pilot-scale shear mixer in the presence of ethyl cellulose. This results in an average flake thickness of ~2 nm, as described in previous work.²⁸, Bioderived CNO powders were synthesized from softwood organosolv lignin (OL) by precarbonization followed by Joule heating. Specifically, the OL was purified by washing with deionized water for 4 h at 90 °C and then precarbonized at 700 °C under N2. The precarbonized OL was milled at 30 Hz for 3 min in a cryo-mill (Retsch) and then mixed with 5% carbon black. The mixture was placed in a quartz tube reactor with copper electrodes for Joule heating with a direct electric current of 4A for 10 min.

Ink Preparation. The graphene ink was prepared by dispersing 10 mg mL $^{-1}$ of the dry graphene/EC powder and 5 mg mL $^{-1}$ of NC in one of two solvent mixtures: 9:9:2 isobutyl acetate/diglyme/Cyrene or 4:4:1:1 isobutyl acetate/diglyme/Cyrene/glycerol. The ink components were added to a vial and ultrasonically agitated overnight. The CNO ink contained 11.25 mg mL $^{-1}$ of CNO

powder, 5 mg mL $^{-1}$ of NC, and 5 mg mL $^{-1}$ of EC in the same solvent mixtures. Premixed composite inks were prepared with different overall solid loadings, using 11.25 mg mL $^{-1}$ CNOs and the appropriate amount of graphene/EC powder based on the sample mixing ratio, which were added to 5 mg mL $^{-1}$ NC and 5 mg mL $^{-1}$ EC and dispersed via ultrasonic agitation in the 4:4:1:1 solvent mixture.

Printing, Post-Processing, and Characterization Instrumentation. All AJP experiments were performed on a custom printing system with a 200 μ m tapered nozzle tip (Nordson, Westlake, OH), a print bed heated to 60 °C, and ink cartridges coupled to a 20 °C cooling circuit. The printer contained three linear motion stages, three mass flow controllers, and two ultrasonic atomizers, along with a custom printhead. The printhead contained an internal helical static mixer to promote aerosol-phase mixing, as described elsewhere. 23,30 All samples were printed onto glass slides. Printed samples were cured in a Lindberg Blue M furnace (Thermo Fisher Scientific, Waltham, MA) using a procedure with a 15 min dwell at 70 °C, a 2 °C min⁻¹ ramp to 325 °C, a dwell at 325 °C for 60 min, and natural cooling based on prior work to decompose polymer dispersants and ensure effective compaction during solvent and polymer removal.³¹ Deposition rate was determined using data collected with a Zygo NewView 9000 optical profilometer (Zygo, Middlefield, CT) and processed using Gwyddion and MATLAB. For this, the deposition rate was determined as the product of the single-pass cross-sectional area and the print speed. Electrical characterization data was collected using a Keithley 2450 source meter in a four-point probe configuration (Keithley, Cleveland, OH). Raman characterization was performed using a Horiba iHR550 (Kyoto, Japan) system equipped with a 532 nm laser operated at 10 mW and a spot size <20 μ m when operated at 50×. Scanning electron microscopy images were obtained using a FEI Quanta 250 FE-SEM (FEI Company, Hillsboro, OR). The Raman data is processed by applying a moving average filter and subtracting a linear baseline. Spectra are normalized to a maximum intensity of 1; the D-peak intensity is taken as the maximum value from 1250-1400 cm⁻¹, and the G peak intensity is taken as the maximum from 1500-1700 cm⁻¹. Raman fitting for carbon nanomaterials can use much more sophisticated methods for better quantitative analysis and physical interpretation of materials.³³ However, due to the complexity of the materials here (containing graphene, CNOs, and polymer residue) and the focus of the results on electrical functionality rather than Raman characteristics, the interpretation of Raman data is limited to this light analysis.

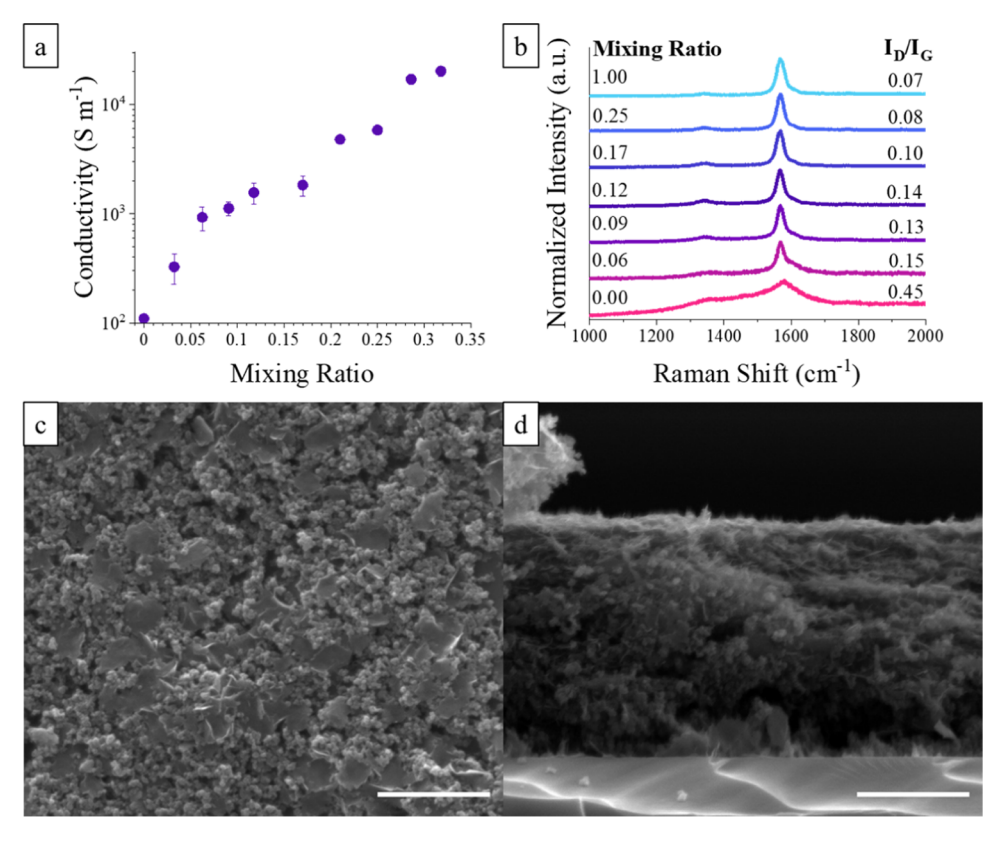


Figure 2. (a) Conductivity data for premixed graphene/CNO inks, including the two individual inks, with graphene conductivity shown as a dashed line. (b) Normalized Raman spectra of a subset of inks with different mixing ratios. (c) Plan view and (d) cross-sectional SEM images of a sample printed on glass obtained from the premixed ink with a mixing ratio of 0.12. Scale bar: 2 μ m.

RESULTS AND DISCUSSION

Materials Benchmarking via Single Ink Printing with **Individual Nanomaterials and Premixed Blends.** Printing characteristics and electrical properties of the graphene and CNO materials, along with discrete blends, were characterized prior to any in situ mixing experiments and graded patterning (Figure 1a). In particular, the deposition rate and electrical properties are key process and performance characteristics, and both were evaluated using a standard toolpath with a resistance test feature (Figure S1). Samples were printed with the 4:4:1:1 inks using carrier gas flow rates ranging from 10-15 sccm to modulate the deposition rate. Following curing, the sample cross section was measured and combined with toolpath information to calculate the deposition rate, corresponding to the volume of film deposited per unit time (Figure 1b). Conductivity values were calculated from the cross-sectional area measurement, sample geometry, and electrical resistance (Figure 1c).

As shown in Figure 1b, both inks exhibit a near-linear increase in deposition rate with carrier gas flow rate (CGFR) above a certain "threshold" flow rate, a relationship commonly observed for AJP.33 While graphene exhibits a slightly higher deposition rate for a given CGFR, both inks have a similar slope and are well matched. This matching is important for downstream efforts to blend the two inks to avoid a significant imbalance of the constituents. As shown in Figure 1c, graphene exhibits a higher electrical conductivity by ~2 orders of magnitude, owing to the high-quality sp² carbon bonding and the 2D morphology that supports efficient packing and flaketo-flake overlap for electrical transport. This desirable morphology is confirmed by SEM, showing printed graphene

traces with a continuous and dense microstructure (Figure 1d). In contrast, the CNOs form films composed of particles featuring more void space and inferior particle-particle contact (Figure 1e).

Following this benchmark characterization of the individual materials, the efficacy of tailoring electrical properties by blending graphene and CNOs was investigated by preparing multiple carbon inks with discrete mixing ratios, which were deposited and analyzed individually. This experimental design allowed the evaluation of conductivity variation between the two end points, approximately 2×10^4 and 10^2 S m⁻¹ for graphene and CNOs, respectively. All inks here were prepared with a 4:4:1:1 solvent ratio of isobutyl acetate, diglyme, Cyrene, and glycerol. For sample notation (Figure 2a), the mixing ratio is defined as the mass percentage of graphene relative to the total mass of graphene and CNOs in the ink.

The experimental results reported in Figure 2a and Table 1 demonstrate the efficacy of mixing carbon nanomaterials to

Table 1. Summary of Discrete Blended Samples, Including I_D/I_G Peak Ratios and Average Conductivity

mixing ratio	$I_{\mathrm{D}}/I_{\mathrm{G}}$	average conductivity (S m ⁻¹)
0.00	0.45	110
0.03	0.28	326
0.06	0.15	926
0.09	0.13	1120
0.12	0.14	1560
0.17	0.10	1830
0.25	0.08	5890
1.00	0.07	20,300

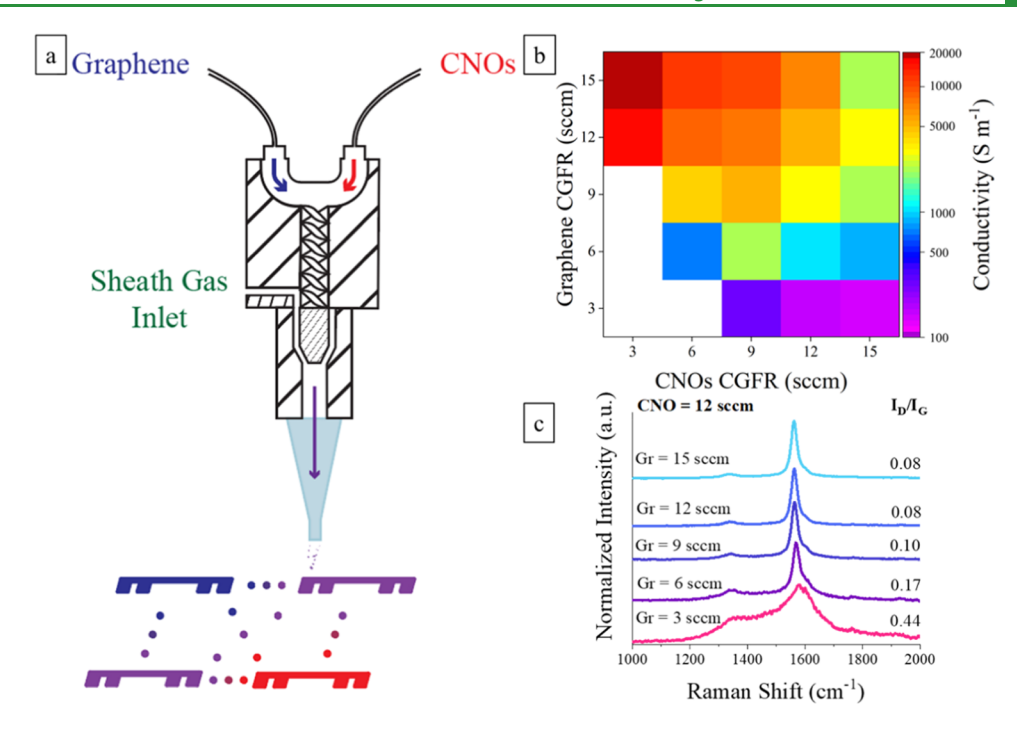


Figure 3. (a) Schematic representation of the multimaterial aerosol jet printing setup, with complete experimental parameters reported in Figure S2c. (b) Heatmap showing conductivity for samples printed with in situ mixing of graphene and CNO inks. White squares are used for samples lacking measurable electrical conductivity. (c) Normalized Raman data for samples printed with a CNO CGFR of 12 sccm and the full range of graphene CGFRs studied.

modulate the electrical properties. For these samples, the conductivity approaches that of pure graphene for mixing ratios exceeding ~0.30. Analysis of these same samples using Raman spectroscopy was performed to evaluate a signature of the chemical composition. The D-to-G peak intensity ratio (I_D/I_G) is a well-established metric to evaluate quality and chemical bonding structure for carbon nanomaterials. 19 Here, a lower I_D/I_G is expected for graphene-rich samples because the G band is an indicator of the in-plane vibration mode for a hexagonal network of carbon atoms, whereas the D signal is related to disruptions in the sp² carbon network and is thus expected to be higher for CNO-rich samples. 19,34 This qualitative behavior is observed, as shown in the Raman data in Figure 2b, with a broad background and high D-peak intensity associated with the CNOs. SEM images corresponding to the mixing ratio of 0.12, including a plan view (Figure 2c) and a cross section (Figure 2d), reveal spherical CNOs randomly dispersed among the graphene flakes, with no clear evidence of material segregation along the sample thickness. We note that the combination of graphene and CNOs is selected for chemical similarity and parallel application utility. As a result, quantitative characterization of mixing is not straightforward, but prior work has evaluated the in-line mixing printhead with more distinct materials to validate the aerosolphase mixing mechanism.²³

The Raman data line up with the material resistivity and reflect the shift from the more disordered, less conductive CNO to high-quality graphene. Specifically, CNO-rich samples exhibit poorly resolved spectra with high $I_{\rm D}/I_{\rm G}$ values (Figure 2b, bottom spectrum), which decrease as more graphene is introduced into the film.

Multimaterial Printing. Following characterization of discrete inks containing well-defined mixtures of the carbon nanomaterials, multimaterial printing was performed by

loading both single-component inks into the printer, atomizing them concurrently, and mixing the generated aerosol droplets from each ink within the printhead during deposition. Mixing aerosols during printing is promoted by a helical static mixer within the printhead (Figure 3a), as shown in previous studies.²³ For these experiments, the 9:9:2 solvent mixture was used, as it results in decreased sensitivity to the deposition rate and in-line drying. This multimaterial printing setup is of particular interest for the additive manufacturing of functionally graded materials since it allows composite patterning with a spectrum of compositions using only two base inks formulated with individual carbon materials. This approach reduces excessive materials waste and time required for evaluating compositions with mixtures formulated up front and provides a versatile capability to tailor composition, and thus properties, during fabrication.⁶

First, a series of samples with unique compositions was prepared by varying the CGFR for each specimen, similar to previous research efforts.²⁰ Specifically, five flow rates of 3, 6, 9, 12, and 15 sccm were used for each ink, resulting in 25 different samples (sheath gas flow rate values in Figure S2). As shown in Figure 3b, this method is effective at modulating the electrical properties. For the CNO-rich sample (15 sccm CNO/3 sccm graphene), the conductivity of 145 S m⁻¹ is a factor of \sim 130 lower than that for the graphene-rich sample (3 sccm CNO/15 sccm graphene), with the overall conductivity decreasing along the matrix diagonal. When moving along the diagonal from bottom-left to top-right, the conductivity remains more consistent (Figure 3b), reflecting a more consistent chemical composition, with the primary difference being the amount of material deposited, as shown by the deposition rate data (Figure S2a). The combination of conductivity and thickness (related to the deposition rate) leads to the sheet resistance for each sample. Therefore, by

changing both conductivity and thickness, the sheet resistance can span nearly 2 orders of magnitude from 54 to 4580 Ω (Figure S2b). Notably, to achieve this same span with just graphene would require samples with thicknesses of 912 to 10.8 nm, which would present challenges for uniformity of more resistive samples. For the CNO ink, samples with thicknesses ranging from 168 to 1.98 μ m would be required to target the same sheet resistance range, with the thicker films more susceptible to mechanical failure and processing challenges (i.e., cracking, adhesion). This illustrates why grading material properties, rather than just thickness, is important, and extending this to more diverse functionality (i.e., semiconductors) can support unique properties that cannot be re-created with a single material.

Raman spectra for samples deposited using a CNO CGFR of 12 sccm and all 5 CGFRs for graphene show a decreasing I_D $I_{\rm G}$ ratio with an increasing graphene CGFR (Table 2). This

Table 2. I_D/I_G Ratio from the Raman Spectra Shown in Figure 3c and the Electrical Conductivity of the Corresponding Films

$y (S m^{-1})$
± 2
<u>+</u> 11
± 27
± 60
± 79

validates the assumption that the CGFR ratio of graphene/ CNO alters the material composition and aligns with the data analyzed for premixed inks (Figure 2c). 19 The correspondence between Raman signals and electrical conductivity for premixed inks matches that for in-line mixing (Figure S2d), and the morphology of samples prepared with in-line mixing (Figure S3) matches that of Figure 2c, confirming the functional similarity between premixed and in-line mixed

In addition to individual samples with tunable but uniform compositions, the same multimaterial AJP setup was applied to fabricate a sample with graded composition by changing the CGFRs of both CNOs and graphene in small increments during manufacturing. Specifically, a 6 mm × 40 mm specimen was manufactured with the CNO CGFR ranging from 15 to 3 sccm while the graphene CGFR varied from 3 to 15 sccm. The toolpath used for this is illustrated in Figure S4 and includes a CGFR variation of 0.03 sccm for every other infill step (50 μ m for each step, thus every 100 μ m), so that the combined CGFR remained constant at 18 sccm, while the sheath gas flow rate was kept at 30 sccm during the print. With these operational parameters, the sample was deposited on glass using a feed rate of 5 mm s⁻¹ and postprocessed using the previously described procedure. The resulting specimen, shown in Figure 4a, was characterized by optical profilometry and current-voltage measurements to evaluate the sample thickness and electrical resistance, respectively.

Thickness data, shown in Figure 4b, are reported as the average height measured for a 1 mm wide sample slice, and resistance data (Figure 4c) were measured every mm using an in-line four-point probe measurement with 1 mm probe spacing (Figure S5). These measurements allowed the calculation of an estimated conductivity using the following equation applicable to a sample with uniform thickness and composition

$$\sigma = \left(\frac{\pi \Delta V}{\ln{(2)I}}t\right)^{-1}$$

with t being the sample thickness, I the current, and ΔV the voltage difference. We note that these extracted conductivities are simply an estimate, since the sample geometry varies from the traditional 4-point probe specimen. Moreover, nonuniform thickness and composition complicate one-to-one mapping of electrical characteristics. Nevertheless, using this approximate relationship, the conductivity starts initially at \sim 150 S m⁻¹ and sharply increases for the first 10 mm of the sample. This trend aligns with the rapid increase in conductivity as graphene is introduced from the fixed-composition control samples (Figure 2a). Beyond this point, the rate at which the estimated conductivity changes decreases, with the maximum measured value being $\sim 17,000 \text{ S m}^{-1}$ at x = 39 mm. This value is likely lower than the value for a graphene-only film due to the significant deviation of the test geometry from a uniform thin film with infinite expanse. The reduced rate in conductivity increase observed for x > 10 mm suggests the material is reaching mixing ratios close to ~ 0.2 , a value where graphene tends to dominate electrical characteristics over the contribution from CNOs, as observed in Figure 2a. Finally, Raman spectroscopy at 1 mm increments was performed, revealing an evolution in I_D/I_G that is well correlated with the change in electrical properties, in agreement with Figures 2b and 3c. In general, the Raman signature exhibits greater variability than electrical, which is attributed to the localized nature of the measurement, the polydispersity in the chemical signature of the CNO material itself, and analysis of the Raman data. As the graphene content increases, this variance is reduced, reflecting the higher purity and more consistent quality of the nanomaterial.

The validation of this capability to smoothly grade properties has broad implications for electronics printing. Carbon nanomaterials were selected for this work due to their applicability in electrochemical systems,³⁵ for which spatially tailoring electrical, chemical, and mass transfer characteristics provides improved design freedom for advanced configurations. Moreover, graded materials offer utility for tailoring interactions with electromagnetic radiation. Just as grading effective refractive index can support advanced optics design (i.e., antireflection functionality), spatially controlling electrical and dielectric properties can modulate interaction with radio frequency electromagnetic waves.³⁶ Extending this capability to a more diverse suite of materials will support broad applications for which the precision and control of additive methods provide unique advantages.

CONCLUSIONS

This work demonstrates the fabrication of functionally graded carbon nanomaterial patterns using a multimaterial AJP technology. To broadly modulate electrical properties during fabrication, two carbon allotropes, namely, graphene and CNOs, were selected as candidate materials due to their combination of similar surface/colloid chemistry and distinct electrical conductivity. Following parallel ink formulation for the two constituent materials, the ability to modulate the electrical properties was evaluated. Different mass ratios of carbon nanomaterials were blended in discrete composite inks

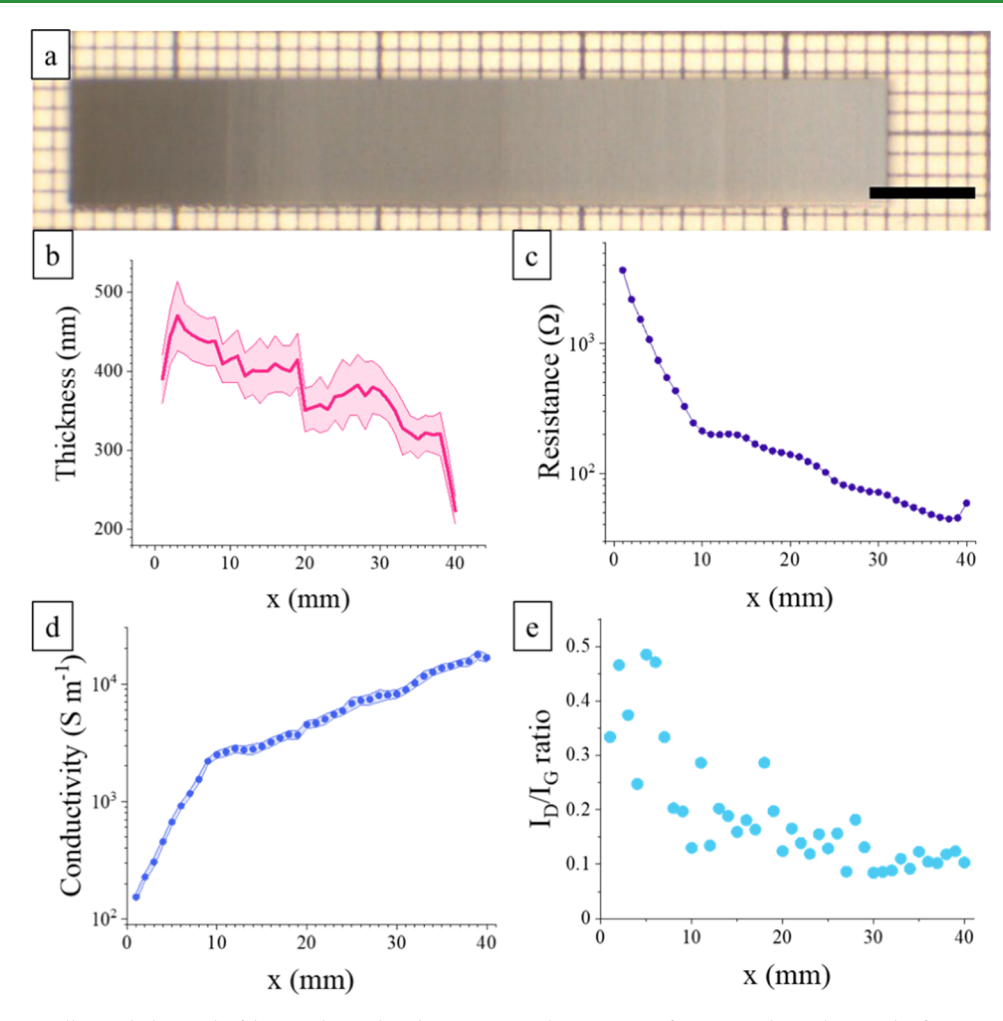


Figure 4. (a) Functionally graded sample fabricated on glass by sweeping the CGFRs of CNO and graphene inks from 15-3 and 3-15 sccm, respectively (left to right); scale bar: 5 mm. (b) Thickness, (c) resistance, (d) estimated conductivity, and (e) Raman I_D/I_C , plotted as a function of position along the sample (position 0 corresponds to 15 sccm CNO/3 sccm graphene). Shaded regions in parts b and (d) indicate a single standard deviation above and below the mean value.

and printed, revealing conductivity values varying continuously between ~100 and ~20,000 S m⁻¹. Then, multimaterial printing was demonstrated for manufacturing of composite samples via in situ mixing, allowing the composition, and thus properties, to be tailored over a wide range from only two precursor inks. Finally, more complex printing control with varying flow rates allowed the fabrication of laterally graded films. The resulting sample exhibits spatially varying electrical properties, establishing a viable method to tune electronic functionality not possible in a single material by exploiting the precision and digital control of printed electronics technologies. This fabrication platform, applied to electronic devices, expands design freedom for applications benefiting from properties not accessible via conventional methods, such as electromagnetic shielding, electrochemical systems, biointegrated materials, and mechanical interfaces.

ASSOCIATED CONTENT

Supporting Information

The Supporting Information is available free of charge at https://pubs.acs.org/doi/10.1021/acsami.3c15088.

> Additional toolpath information and additional characterization of printed samples (PDF)

AUTHOR INFORMATION

Corresponding Author

Ethan B. Secor – Department of Mechanical Engineering, Iowa State University, Ames, Iowa 50010, United States; orcid.org/0000-0003-2324-1686; Email: esecor@ iastate.edu

Authors

Livio Gamba - Department of Mechanical Engineering, Iowa State University, Ames, Iowa 50010, United States Moham Ed Abdur Razzaq - Department of Mechanical

Engineering, Iowa State University, Ames, Iowa 50010, United States

Santiago Diaz-Arauzo - Department of Materials Science and Engineering, Northwestern University, Evanston, Illinois 60208, United States

Mark C. Hersam – Department of Materials Science and Engineering, Northwestern University, Evanston, Illinois 60208, United States; Department of Chemistry, Northwestern University, Evanston, Illinois 60208, United States; Department of Electrical and Computer Engineering, Northwestern University, Evanston, Illinois 60208, United States; orcid.org/0000-0003-4120-1426

Xianglan Bai — Department of Mechanical Engineering, Iowa State University, Ames, Iowa 50010, United States; o orcid.org/0000-0001-6849-2687

Complete contact information is available at: https://pubs.acs.org/10.1021/acsami.3c15088

Author Contributions

The manuscript was written through contributions of all authors. All authors have given approval to the final version of the manuscript.

Notes

The authors declare no competing financial interest.

ACKNOWLEDGMENTS

L.G. and E.B.S. acknowledge Northrop Grumman NG Next Research Laboratories for funding support, the National Science Foundation under NSF CMMI-2224303, and the ISU Mechanical Engineering department for access to characterization equipment. L.G. also gratefully acknowledges Amin Karamati and Mahya Rahbar for their assistance with Raman spectroscopy, and Dr. Xinwei Wang of ISU for access to Raman spectroscopy facilities. M.E.A.R. and X.B. acknowledge the Iowa Energy Center (20-IEC-017) for funding support. S.D.-A. and M.C.H. acknowledge support from the National Science Foundation MADE-PUBLIC Future Manufacturing Research Grant Program (NSF Award Number CMMI-2037026).

REFERENCES

- (1) Zhang, L. X.; Zhang, B.; Sun, Z.; Pan, X. Y.; Shi, J. M.; Feng, J. C. Preparation of Graded Double-Layer Materials for Brazing C/C Composite and TC4. *J. Alloys Compd.* **2020**, 823, No. 153639.
- (2) Boggarapu, V.; Gujjala, R.; Ojha, S.; Acharya, S.; Venkateswara Babu, P.; Chowdary, S.; Kumar Gara, D. State of the Art in Functionally Graded Materials. *Compos. Struct.* **2021**, 262, No. 113596.
- (3) Pompe, W.; Worch, H.; Epple, M.; Friess, W.; Gelinsky, M.; Greil, P.; Hempel, U.; Scharnweber, D.; Schulte, K. Functionally Graded Materials for Biomedical Applications. *Mater. Sci. Eng., A* **2003**, 362 (1–2), 40–60.
- (4) Müller, E.; Drašar, Č.; Schilz, J.; Kaysser, W. A. Functionally Graded Materials for Sensor and Energy Applications. *Mater. Sci. Eng.,* A 2003, 362 (1–2), 17–39.
- (5) Bharti, I.; Gupta, N.; Gupta, K. M. Novel Applications of Functionally Graded Nano, Optoelectronic and Thermoelectric Materials. *Int. J. Mater., Mech. Manuf.* **2013**, 221–224.
- (6) Craton, M. T.; Albrecht, J. T.; Chahal, P.; Papapolumerou, J. In Situ Nanocomposite Fabrication for RF Electronics Applications with Additive Manufacturing. *IEEE Trans. Microwave Theory Tech.* **2020**, 68 (5), 1646–1659.
- (7) Pu, J.; Li, J.; Zhang, K.; Zhang, T.; Li, C.; Ma, H.; Zhu, J.; Braun, P. V.; Lu, J.; Zhang, H. Conductivity and Lithiophilicity Gradients Guide Lithium Deposition to Mitigate Short Circuits. *Nat. Commun.* **2019**, *10* (1), No. 1896.
- (8) Craton, M. T.; Albrecht, J. D.; Chahal, P.; Papapolymerou, J. Multimaterial Aerosol Jet Printed Magnetic Nanocomposites for Microwave Circuits. *IEEE Trans. Compon., Packag., Manuf. Technol.* **2021**, *11* (5), 865–871.
- (9) Saleh, B.; Jiang, J.; Fathi, R.; Al-hababi, T.; Xu, Q.; Wang, L.; Song, D.; Ma, A. 30 Years of Functionally Graded Materials: An Overview of Manufacturing Methods, Applications and Future Challenges. *Composites, Part B* **2020**, 201, No. 108376.
- (10) Goyal, R. K.; Katkade, S. S.; Mule, D. M. Dielectric, Mechanical and Thermal Properties of Polymer/BaTiO3 Composites for Embedded Capacitor. *Composites, Part B* **2013**, 44 (1), 128–132.

- (11) Sarathchandra, D. T.; Kanmani Subbu, S.; Venkaiah, N. Functionally Graded Materials and Processing Techniques: An Art of Review. *Mater. Today Proc.* **2018**, *5* (10), 21328–21334.
- (12) Groves, J. F.; Wadley, H. N. G. Functionally Graded Materials Synthesis via Low Vacuum Directed Vapor Deposition. *Composites, Part B* **1997**, 28 (1–2), 57–69.
- (13) Nemat-Alla, M. M.; Ata, M. H.; Bayoumi, M. R.; Khair-Eldeen, W. Powder Metallurgical Fabrication and Microstructural Investigations of Aluminum/Steel Functionally Graded Material. *Mater. Sci. Appl.* **2011**, *02* (12), 1708–1718.
- (14) Kieback, B.; Neubrand, A.; Riedel, H. Processing Techniques for Functionally Graded Materials. *Mater. Sci. Eng., A* **2003**, 362 (1–2), 81–106.
- (15) Ou, C.; Zhang, L.; Jing, Q.; Narayan, V.; Kar-Narayan, S. Compositionally Graded Organic—Inorganic Nanocomposites for Enhanced Thermoelectric Performance. *Adv. Electron. Mater.* **2020**, 6 (1), No. 1900720.
- (16) Zeng, M.; Du, Y.; Jiang, Q.; Kempf, N.; Wei, C.; Bimrose, M. V.; Tanvir, A. N. M.; Xu, H.; Chen, J.; Kirsch, D. J.; Martin, J.; Wyatt, B. C.; Hayashi, T.; Saeidi-Javash, M.; Sakaue, H.; Anasori, B.; Jin, L.; McMurtrey, M. D.; Zhang, Y. High-Throughput Printing of Combinatorial Materials from Aerosols. *Nature* **2023**, *617* (7960), 292–298.
- (17) Obata, K.; Schonewille, A.; Slobin, S.; Hohnholz, A.; Unger, C.; Koch, J.; Suttmann, O.; Overmeyer, L. Hybrid 2D Patterning Using UV Laser Direct Writing and Aerosol Jet Printing of UV Curable Polydimethylsiloxane. *Appl. Phys. Lett.* **2017**, *111* (12), No. 121903.
- (18) Lekshmi, D. R.; Adarsh, S. P.; Bayal, M.; Nair, S. S.; Surendran, K. P. Functionally Graded Magnetodielectric Composite Substrates for Massive Miniaturization of Microstrip Antennas. *Mater. Adv.* **2022**, 3 (5), 2380–2392.
- (19) Rasel, S.; Bhatkar, O.; Smith, D.; Kowal, M. D.; Anderson, M.; Rizvi, R.; Kaner, R. B. Self-Assembled Functionally Graded Graphene Films with Tunable Compositions and Their Applications in Transient Electronics and Actuation. ACS Appl. Mater. Interfaces 2019, 11 (26), 23463–23473.
- (20) Wang, K.; Chang, Y.-H.; Zhang, C.; Wang, B. Conductive-on-Demand: Tailorable Polyimide/Carbon Nanotube Nanocomposite Thin Film by Dual-Material Aerosol Jet Printing. *Carbon* **2016**, *98*, 397–403.
- (21) Gamba, L.; Johnson, Z. T.; Atterberg, J.; Diaz-Arauzo, S.; Downing, J. R.; Claussen, J. C.; Hersam, M. C.; Secor, E. B. Systematic Design of a Graphene Ink Formulation for Aerosol Jet Printing. ACS Appl. Mater. Interfaces 2023, 15 (2), 3325–3335.
- (22) Mykhailiv, O.; Zubyk, H.; Plonska-Brzezinska, M. E. Carbon Nano-Onions: Unique Carbon Nanostructures with Fascinating Properties and Their Potential Applications. *Inorg. Chim. Acta* **2017**, 468, 49–66.
- (23) Gamba, L.; Lajoie, J. A.; Sippel, T. R.; Secor, E. B. Multi-Material Aerosol Jet Printing of Al/Cuo Nanothermites for Versatile Fabrication of Energetic Antennas. *Adv. Funct. Mater.* **2023**, *33*, No. 2304060.
- (24) Shabana, Y. M.; Tarek, D.; Samir, S.; Gaber, S. A.; Amer, S. M.; Shaban, A. M.; Ibrahim, M. A. A.; Elfaramawy, M. O.; Ibrahim, M. O. M.; El Qassim, M.; Abdelhamid, N. M. In *Enhancing the Performance of Biosensors Using Advanced Materials*, 2022 4th Novel Intelligent and Leading Emerging Sciences Conference (NILES); IEEE: Giza, Egypt, 2022; pp 151–154.
- (25) Shabana, Y. M.; Samy, M. A.; Abdel-Aziz, M. A.; Hindawi, M. E.; Mosry, M. G.; Albarawy, A.-R. M.; Omar, M. M.; Mohamed, A. A.; Attia, A. A. Enhancing the Performance of Micro-Biosensors by Functionally Graded Geometrical and Material Parameters. *Arch. Appl. Mech.* **2021**, *91* (6), 2497–2511.
- (26) Di Novo, N. G.; Cantù, E.; Tonello, S.; Sardini, E.; Serpelloni, M. Support-Material-Free Microfluidics on an Electrochemical Sensors Platform by Aerosol Jet Printing. Sensors 2019, 19 (8), 1842. (27) Zhao, D.; Liu, T.; Zhang, M.; Liang, R.; Wang, B. Fabrication and Characterization of Aerosol-Jet Printed Strain Sensors for

- Multifunctional Composite Structures. Smart Mater. Struct. 2012, 21 (11), No. 115008.
- (28) Secor, E. B.; Prabhumirashi, P. L.; Puntambekar, K.; Geier, M. L.; Hersam, M. C. Inkjet Printing of High Conductivity, Flexible Graphene Patterns. *J. Phys. Chem. Lett.* **2013**, *4*, 1347–1351.
- (29) Downing, J. R.; Diaz-Arauzo, S.; Chaney, L. E.; Tsai, D.; Hui, J.; Seo, J. T.; Cohen, D. R.; Dango, M.; Zhang, J.; Williams, N. X.; Qian, J. H.; Dunn, J. B.; Hersam, M. C. Centrifuge-Free Separation of Solution-Exfoliated 2D Nanosheets via Cross-Flow Filtration. *Adv. Mater.* **2023**, 35 (24), No. 2212042.
- (30) Secor, E. B. In-Line Mixing Printhead for Multimaterial Aerosol Jet Printing. U.S. Patent US11220112B2, Jan 11, 2022.
- (31) Gamba, L.; Diaz-Arauzo, S.; Hersam, M. C.; Secor, E. B. Aerosol Jet Printing of Phase-Inversion Graphene Inks for High-Aspect-Ratio Printed Electronics and Sensors. *ACS Appl. Nano Mater.* **2023**, *6*, 21133.
- (32) Jorio, A.; Souza Filho, A. G. Raman Studies of Carbon Nanostructures. *Annu. Rev. Mater. Res.* **2016**, *46* (1), 357–382.
- (33) Secor, E. B. Principles of Aerosol Jet Printing. Flex. Print. Electron 2018, 20183, No. 035002.
- (34) Wang, M.; Duong, L. D.; Oh, J.-S.; Mai, N. T.; Kim, S.; Hong, S.; Hwang, T.; Lee, Y.; Nam, J.-D. Large-Area, Conductive and Flexible Reduced Graphene Oxide (RGO) Membrane Fabricated by Electrophoretic Deposition (EPD). ACS Appl. Mater. Interfaces 2014, 6 (3), 1747–1753.
- (35) Fapanni, T.; Sardini, E.; Serpelloni, M.; Tonello, S. Nano-Functionalized Electrochemical Sensors by Aerosol Jet Printing. *IEEE Sens. J.* **2022**, 22 (22), 21498–21507.
- (36) Shamshirgar, A. S.; Rojas Hernández, R. E.; Tewari, G. C.; Fernández, J. F.; Ivanov, R.; Karppinen, M.; Hussainova, I. Functionally Graded Tunable Microwave Absorber with Graphene-Augmented Alumina Nanofibers. *ACS Appl. Mater. Interfaces* **2021**, *13* (18), 21613–21625.